



## On the Use of the H/V Spectral Ratio Method to Estimate the Fundamental Frequency of Tailings Dams

César Pastén, G. Peña, D. Comte, L. Díaz, J. Burgos & A. Rietbrock

To cite this article: César Pastén, G. Peña, D. Comte, L. Díaz, J. Burgos & A. Rietbrock (2022): On the Use of the H/V Spectral Ratio Method to Estimate the Fundamental Frequency of Tailings Dams, Journal of Earthquake Engineering, DOI: [10.1080/13632469.2022.2087799](https://doi.org/10.1080/13632469.2022.2087799)

To link to this article: <https://doi.org/10.1080/13632469.2022.2087799>



Published online: 29 Aug 2022.



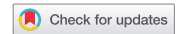
Submit your article to this journal [↗](#)



View related articles [↗](#)



View Crossmark data [↗](#)



# On the Use of the H/V Spectral Ratio Method to Estimate the Fundamental Frequency of Tailings Dams

César Pastén<sup>a</sup>, G. Peña<sup>b</sup>, D. Comte<sup>c</sup>, L. Díaz<sup>d</sup>, J. Burgos<sup>d</sup>, and A. Rietbrock<sup>e</sup>

<sup>a</sup>Department of Civil Engineering and Advanced Mining Technology Center (AMTC), University of Chile, Santiago, Chile; <sup>b</sup>Advanced Mining Technology Center (AMTC), University of Chile, Santiago, Chile; <sup>c</sup>Department of Geophysics and Advanced Mining Technology Center (AMTC), University of Chile, Santiago, Chile; <sup>d</sup>Anglo American, Chile; <sup>e</sup>Department of Geophysics, Karlsruhe Institute of Technology, Karlsruhe, Germany

## ABSTRACT

This paper analyses the feasibility of estimating the fundamental frequency of an 85 m high cycloned-sand tailings dam located in the Central-North area of Chile using the single-station H/V Spectral Ratio Method (HVSr), calculated from seismic ambient noise and earthquakes recorded by a temporal seismic array deployed along the embankment crest, the downstream slope, and the dam toe, directly over the foundation soil. The fundamental vibration frequencies obtained from the HVSr's show consistency with results from the Standard Spectral Ratio method (SSR) calculated between the crest and the toe using the available earthquake records, particularly in the dam central part.

## ARTICLE HISTORY

Received 6 October 2021  
Accepted 21 May 2022

## KEYWORDS

H/V Spectral Ratio; Standard Spectral Ratio; tailings dam; fundamental frequency

## 1. Introduction

Earthquakes are among the most common triggers of tailings dam failures (WISE Uranium Project 2019). Due to the subduction of the Nazca plate beneath the South American plate, Chile is subject to a highly active seismic activity. In the last decades, Central Chile was hit by the 1985 Mw 8.0 Valparaiso, the 2010 Mw 8.8 Maule, and the 2015 Mw 8.3 Illapel Earthquakes (Ruiz and Madariaga 2018). The relationship between the subduction process and mineralization has been recognized in metallogenic studies ever since the theory of plate tectonics was widely accepted. Important metallogenic belts worldwide are mostly located in subduction zones. Porphyry-type deposits are generally related to arc magmatism or partial melting of subducted plates, with ore-forming fluids areas derived from the dehydration of the subducted slab, indicating the intimate relationship between the subduction process and mineralization (e.g. Wilkinson 2013). As a result, Chile has one of the largest copper reserves in the World and is currently one of the largest copper producers. The copper concentration process, when copper sulfide ore is mined, generates large amounts of tailings that must be safely stored in Tailings Storage Facilities (TSF). Villavicencio et al. (2014) reported that 31 out of 38 physical stability failures involving loss of human life, significant environmental damage, and economic losses of Chilean sand tailings dams since 1915 were linked to earthquake loading, which highlights the relevance of understanding the seismic response of these geostructures.

Seismic response of a tailings dam depends upon the geometry and the stiffness of the materials that compose the embankment dam, as well as the input ground motion, among other factors. Materials stiffness can be estimated through the shear and compressional wave velocities, which can be measured in-situ with invasive and non-invasive geophysical techniques. The fundamental vibration frequency is another dynamic parameter that characterizes a dam dynamic behavior (Gazetas 1987). This frequency mainly results from the dam geometry and its material stiffness. An input ground

motion with high energy content around the fundamental frequency may induce resonance of the embankment dam, increase its dynamic displacements, and eventually cause slope instabilities, which may compromise the physical stability of the entire TSF.

In geotechnical earthquake engineering, the most common method to determine the amplification function of a soil deposit is the Standard Spectral Ratio (SSR) method, computed as the spectral ratio between the response at the site of interest with respect to the response of a reference site (Borcherdt 1970). The reference site can be either the base of the soil deposit where the input motion arrives or a reference station that is ideally located on a site not affected by the local soil conditions, either over stiff soil or hard rock. The fundamental vibration frequency is estimated as the lower frequency where the amplification function peaks.

Another simple method that estimates the amplification function is the single-station Horizontal-to-Vertical H/V Spectral Ratio (HVSR) method, also known as the Nakamura's method (Nakamura 1989). This method was originally defined to be used with continuous records of seismic ambient noise, of at least 30 min long for detecting low fundamental frequencies (Bard 2004). It has been proven that the HVSR curves obtained from the processing of seismic ambient noise and earthquake records allow the estimation of the fundamental frequency of soils deposits, implying that the HVSR is a robust method, regardless of the input signal nature (Fernández et al. 2019; Molnar et al. 2018). The validity of the HVSR method has been studied in natural sloped terrains with promising results in the identification of the fundamental vibration frequency (Diaz-Segura 2016), the estimation of topographic amplification (He et al. 2020), and the presence and orientation of the slope directional resonance (Del Gaudio et al. 2014). Cetin et al. (2005) systematically tested the use of the HVSR method in earthfill dams for water storage. This study found discrepancies between the fundamental frequencies gathered from the SSR and the HVSR methods attributed to internal impedance contrasts in the dam and 3D valley effects. To the best of the author's knowledge, the applicability of the HVSR method for the estimation of the fundamental frequency of tailings dams has not been addressed in other studies. Hence, this paper analyses the feasibility of estimating fundamental frequencies of a cycloned sand tailings dam located in a highly active seismic environment using the HVSR method. The HVSR curves are calculated from seismic ambient noise and earthquakes recorded by a temporal seismic array installed over the tailings dam and the foundation soil. The results of the HVSRs are compared with SSRs calculated between the crest and the toe of the dam using available earthquake records, including the 2015 Mw 8.3 Illapel Earthquake.

## 2. Studied Tailings Dam

In this paper, we analyze a sand tailings dam located in the Coastal Mountain Range of Central Chile, at about 100 km northwest of the Santiago capital city and 25 km from the Pacific coast (Fig. 1).

The studied tailings dam was designed for a maximum storage capacity of  $181 \cdot 10^6$  ton of tailings and currently has a  $2.7 \text{ km}^2$  footprint (Fig. 2(a)). The embankment dam was built with cycloned sand following the downstream construction method up to a maximum average height of 60 m, after which the lifting process followed the center-line method at a rising rate of about 2 m/year. The cycloned sand, classified as a silty sand (SM) according to the Unified Soil Classification System (USCS), is hydraulically placed from the crest of the embankment dam towards the downstream slope following a north-to-south abutment construction sequence. After a 15 cm layer of sand is deposited in the embankment, the layer is compacted with several passes of a mechanical roller compactor to achieve around 90% of the maximum dry density obtained from the Standard Proctor Test. The average dry density of the embankment obtained with this method is approximately  $17 \text{ ton/m}^3$  (Valenzuela 2016). A representative cross-section near the tallest zone of the dam is shown in Fig. 2(b). The current downstream slope, measured as a horizontal to vertical ratio (H:V), is  $H:V = 3.5:1$ , a gentle slope compared to embankment dams built from borrowed materials, which can reach slopes as steep as  $H:V = 2:1$ .

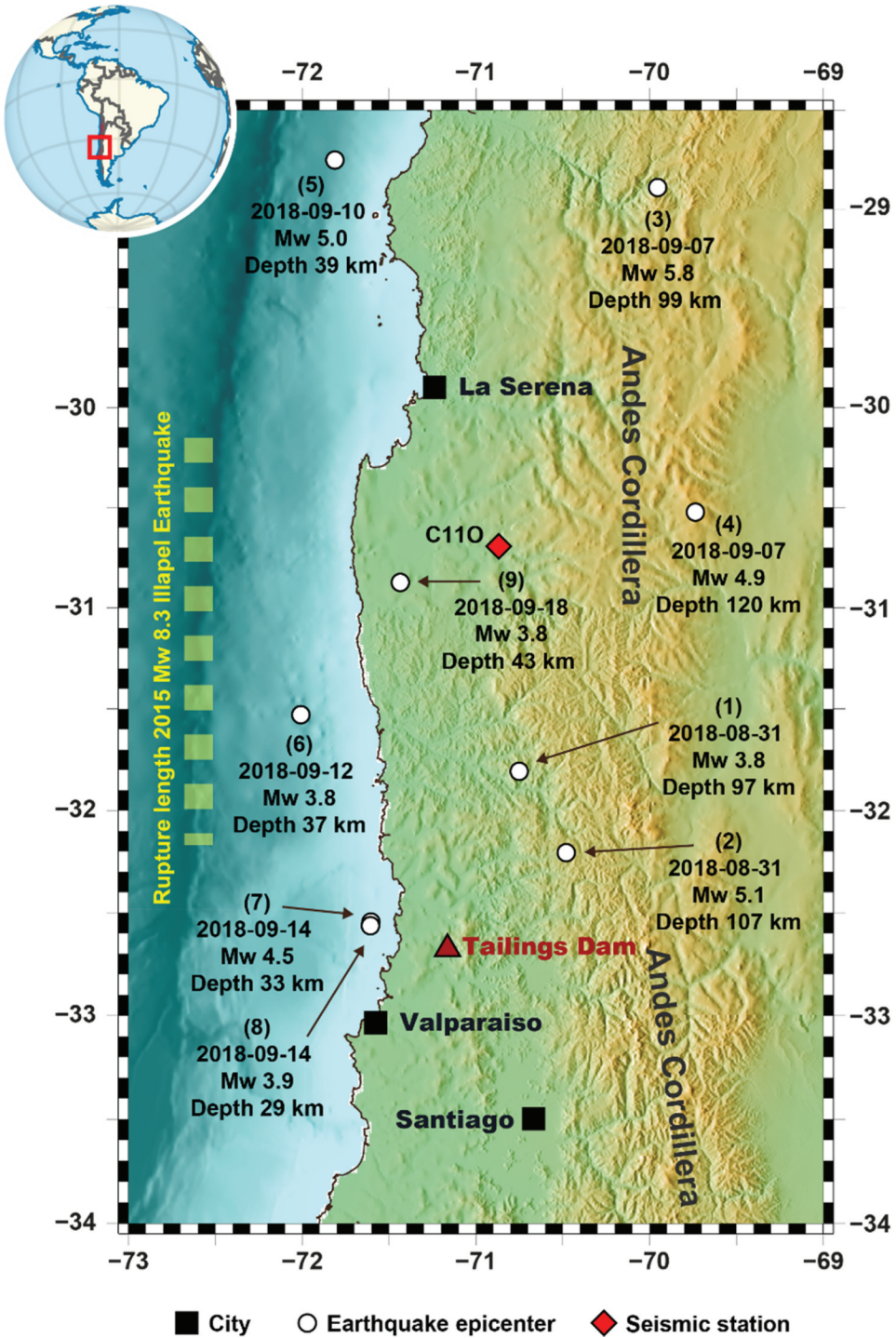
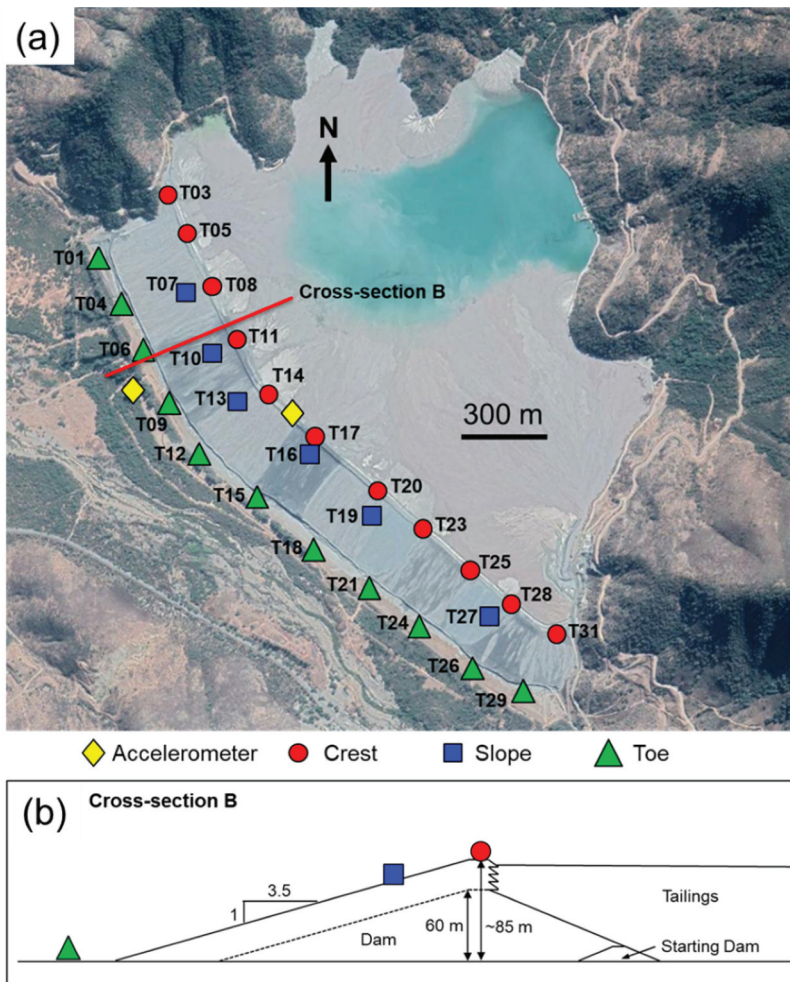


Figure 1. Location of the studied Tailings Dam in Central-North Chile. The epicenter and information of the earthquakes recorded by the seismic array are also shown. The rupture length of the 2015 Mw 8.3 Illapel Earthquake is based on Fernández et al. (2019). The red square in the inset shows the location of Central-North Chile.



**Figure 2.** Seismic array deployed over the tailings dam. (a) Plan view of the tailings storage facility (Google Earth) and (b) cross-section B of the embankment dam. Triangles, circles, and squares represent the location of the temporal array of seismic stations whereas diamonds represent the location of accelerometers that recorded the 2015 Mw 8.3 Illapel Earthquake.

Geological reports indicate that the location site of the tailings dam contains alluvial soils composed of gravels, clays, and sands. According to borings and test pits, 12-inch boulders can be found in some areas. In other areas, low plasticity clays and clayey sands can be concentrated. Seismic refraction tests and geotechnical borings show that the bedrock depth averages 70 m underneath the crest of the dam, but it can reach up to 90 m near the toe. Multi-Channel Analysis of Surface Waves method (MASW) tests performed at the toe of the dam indicate that the shear wave velocity of the shallower 30 m ranges from 300 to 450 m/s.

The study area is exposed to large interplate, intraplate and shallow crustal earthquakes. During the last five decades, this region has been affected by the intraplate 1965 Mw 7.4 and the interplate 1971 Mw 7.8 La Ligua Earthquakes, the interplate 1985 Mw 8.0 Valparaiso Earthquake, and most recently by the interplate 2015 Mw 8.3 Illapel Earthquake (Ruiz and Madariaga 2018).

The studied tailings dam is 2 km north of El Cobre N°1 tailings dam, built following an upstream construction method and failed due to seismically-induced liquefaction after the intraplate 1965 Mw 7.4 La Ligua Earthquake, causing more than 200 casualties and widespread contamination of the downstream agricultural valley (Dobry and Alvarez 1967). This failure highlights the devastating consequences of the physical instability of these dams during large subduction earthquakes.

The 2015 Illapel Earthquake (rupture length shown in Fig. 1) did not cause damage in the studied tailings dam. Accelerometers installed in the crest and the toe of the embankment (yellow diamonds in Fig. 2) recorded maximum horizontal accelerations of 0.11 g and 0.06 g, respectively (Verdugo et al. 2017). The maximum peak ground acceleration recorded by the National Seismological Center for this earthquake was 0.83 g in the station C110 Monte Patria (Fernández et al. 2019), located 215 km north of the studied tailings dam (see Fig. 1).

### 3. Temporal Seismic Array

The seismic array installed in the studied tailings dam consisted of 28 stations, each one equipped with a short period 3-component 4.5 Hz geophone, an Omnirecs DataCube3 Ext datalogger recording 200 samples per second, a GPS antenna for time synchronization, and a sealed gel deep cycle battery. The stations recorded continuously from August 29, 2018 to September 26, 2018. Figure 2 shows a plan view with the location of the 28 seismic stations deployed in the tailings dam. Eleven stations were installed in the crest of the embankment dam (red circles in Figure 2), 6 installed in the downstream slope (blue squares in Figure 2), and 11 installed at the downstream slope toe on top of the foundation soil (green triangles in Figure 2). The last group of stations were deployed at an average distance of 5 m apart from the embankment dam due to constraints of the underground infrastructure. The stations were buried in a sealed plastic container and the GPS antennas were raised 50 cm above the surface.

Figure 3 shows an example of the daily continuous record of the station T08 in the vertical component. The amplitude of the velocity time history (Fig. 3(a)) increases during the time of the day when the tailings facility operates, between 9 am and 6 pm. Figure 3(b) shows a normalized spectrogram with the frequency content of the time history signal. The frequency content remains relatively constant before the operation starts working at the tailings dam (stationary seismic ambient noise in Fig. 3(a)). However, the frequency content changes considerably between 3 and 20 Hz during operation hours.

At least 9 earthquakes of different magnitude were recorded by the seismic stations during the period when the seismic array was under operation. The earthquakes moment magnitudes ( $M_w$ ) ranged from 3.8 to 5.8 and the epicentral distances vary from 10 to 410 km. The epicenter of the earthquakes along with their dates, magnitudes, and depths are shown in Fig. 1 and Table 1. Table 2 shows the earthquake records in each station set for calculating the SSR and HVSR.

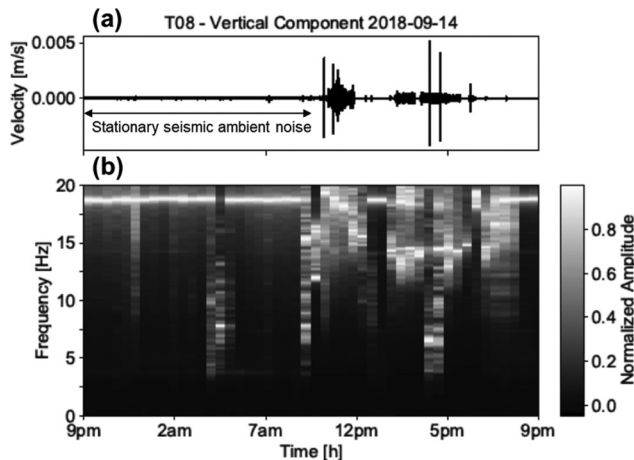


Figure 3. Example of a continuous daily record at station T08 in the vertical component (September 14, 2018). (a) Velocity time history and (b) normalized spectrogram.

**Table 1.** Recorded earthquakes.

Earthquake	Date and time (UTC)	Latitude (°)	Longitude (°)	Depth (Km)	Moment Magnitude (Mw)
1	2018-08-31 10:26:44	-31.811	-70.650	97	3.8
2	2018-08-31 13:25:01	-32.234	-70.489	107	5.1
3	2018-09-07 02:39:17	-28.917	-70.181	99	5.8
4	2018-09-07 23:12:47	-30.470	-69.925	120	4.9
5	2018-09-10 08:24:11	-28.793	-71.547	39	5.0
6	2018-09-12 19:31:14	-31.554	-71.836	37	3.8
7	2018-09-14 18:15:11	-32.524	-71.592	33	4.5
8	2018-09-14 18:46:51	-32.526	-71.592	29	3.9
9	2018-09-18 23:50:10	-30.848	-71.334	43	3.8

**Table 2.** Earthquakes and number of days recorded in the seismic stations.

Station	Earthquake									Recorded days
	1	2	3	4	5	6	7	8	9	
T01	Y	Y	Y	Y	Y					27
T04	Y	Y	Y		Y	Y	Y	Y		27
T05	Y	Y	Y	Y	Y					27
T06			Y	Y	Y	Y	Y			27
T07			Y	Y	Y	Y	Y	Y		25
T08	Y	Y	Y		Y	Y	Y	Y		27
T09	Y	Y	Y	Y	Y	Y	Y	Y		27
T11	Y	Y	Y	Y	Y	Y	Y	Y		27
T12			Y	Y	Y	Y	Y	Y		27
T13			Y	Y	Y	Y	Y	Y		25
T14			Y	Y	Y	Y	Y	Y		27
T15			Y	Y	Y	Y	Y	Y	Y	27
T16			Y	Y	Y	Y	Y	Y	Y	25
T17			Y	Y	Y	Y	Y	Y	Y	27
T18			Y	Y	Y	Y	Y	Y	Y	27
T19					Y	Y	Y	Y	Y	24
T20					Y	Y	Y	Y	Y	27
T21	Y	Y				Y	Y	Y	Y	23
T23	Y	Y				Y	Y	Y	Y	27
T24	Y	Y	Y	Y	Y	Y	Y	Y	Y	27
T25	Y	Y	Y	Y	Y	Y	Y	Y	Y	27
T26			Y	Y	Y		Y	Y	Y	27
T27			Y	Y	Y		Y	Y	Y	21
T28			Y	Y	Y		Y	Y	Y	26
T29			Y	Y			Y	Y	Y	27
T31			Y	Y			Y	Y	Y	25

Note. "Y" means that the earthquake was recorded by the station

Figure 4 shows examples of velocity records of earthquake #7 (Fig. 1) in stations located in the crest, the downstream slope, and the toe. The records highlight the amplification of stations in the slope and crest in relation to the strong motion recorded at the toe.

## 4. Methodology

### 4.1. Standard Spectral Ratios (SSR)

Standard Spectral Ratios SSR were calculated from earthquakes recorded in the stations at the crest, in relation to the stations at the dam's toe. The records in the NS and EW directions were projected into two perpendicular directions: a longitudinal direction (L) along the crest axis and a transverse direction (T) along a cross-section of the dam (e.g. cross-section B in Fig. 2(a)).

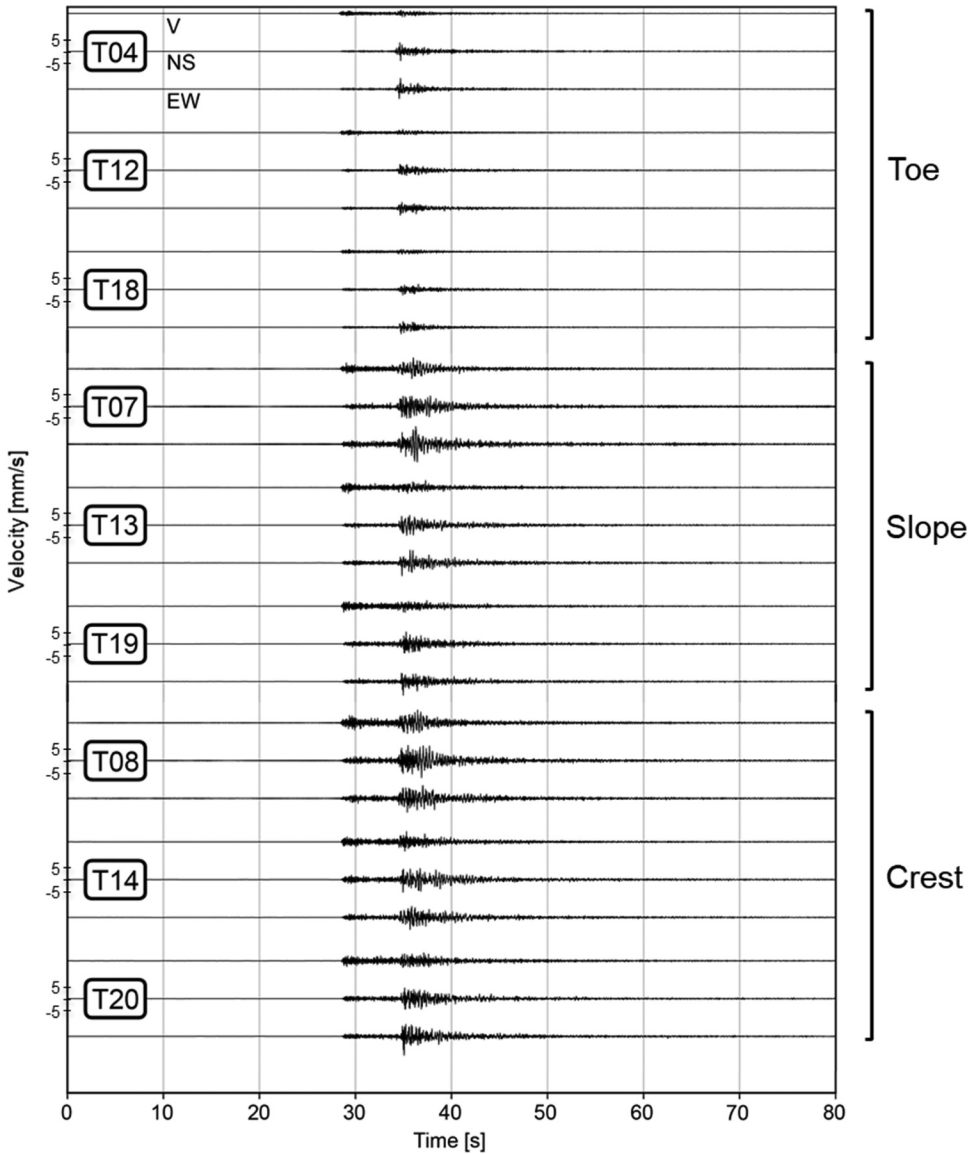


Figure 4. Velocity records of earthquake #7 (epicenter shown in Fig. 1 and details in Table 1) in stations located in the crest, the downstream slope, and the dam toe. V: Vertical, NS: North-south, and EW: east-west directions.

Table 3 shows the station pairs and earthquake records considered in the calculation of the SSR. The station pairs were chosen in such a way that the stations in the crest and in the downstream slope toe were installed in the same cross-section of the dam.

SSR calculation consisted of selecting a 2 minutes window centered in the signal maximum amplitude (e.g. see Fig. 4). Then, the amplitude Fourier spectra of the velocity records were calculated in each direction and smoothed with a running average window of 0.5 Hz bandwidth. The ratio between the smoothed Fourier amplitudes were computed in the T, L, and vertical directions. Finally, the standard spectral ratios of the analyzed earthquakes were averaged for every station pair.

**Table 3.** Station pairs and earthquakes considered in the calculation of SSR.

Station Pair	Earthquake								
	1	2	3	4	5	6	7	8	9
T05-T01	Y	Y	Y	Y	Y				
T08-T04	Y	Y	Y		Y	Y	Y	Y	
T11-T09	Y	Y	Y	Y	Y	Y	Y	Y	
T14-T12			Y	Y	Y	Y	Y	Y	
T17-T15			Y	Y	Y	Y	Y	Y	Y
T20-T18			Y	Y	Y	Y	Y	Y	Y
T23-T21	Y	Y				Y	Y	Y	Y
T25-T24	Y	Y	Y	Y	Y	Y	Y	Y	Y
T28-T26			Y	Y	Y		Y	Y	Y
T31-T29			Y	Y			Y	Y	Y
T07-T06			Y	Y	Y	Y	Y		
T13-T12			Y	Y	Y	Y	Y	Y	
T16-T15			Y	Y	Y	Y	Y	Y	Y
T19-T18			Y	Y	Y	Y	Y	Y	Y
T27-T26			Y	Y	Y		Y	Y	Y

Note. "Y" means that the earthquake was recorded by the station pair

## 4.2. Horizontal to Vertical Spectral Ratios (HVSr)

### 4.2.1. HVSr from Earthquake Records (eHVSr)

The earthquakes recorded by the seismic array were used to calculate single-station eHVSr. First, the amplitude Fourier spectra of the velocity records in the T, L, and vertical directions defined for the calculation of the SSR were calculated and smoothed with a running average window of 0.5 Hz bandwidth. Then, the spectra of the horizontal directions (T and L), as well as their square average, were divided by the vertical component. For every evaluated frequency in each station, the mean value was calculated.

### 4.2.2. HVSr from Seismic Ambient Noise Records (mHVSr)

Single-station mHVSr were calculated using 12 hours of stationary seismic ambient noise recorded from 9 pm to 9 am, before the beginning of the TSF operation (Fig. 3(a)). We followed the methodology described in Pastén et al. (2016), using 30s windows automatically selected from the amplitude STA/LTA ratio between 0.5 and 2.0, with a short time period  $t_{STA} = 1$  s, and a long time period  $t_{LTA} = 60$ s. The horizontal component was calculated as the squared average of the T and L directions in the frequency domain. The calculations were performed using the open-source Geopsy software ([www.geopsy.org](http://www.geopsy.org)).

## 5. Results

Figure 5 shows an example of the SSR computed for the station pair T14-T12 in the L, T, and vertical directions. The thick curve was computed as the average of the six recorded earthquakes (see the earthquakes considered in Table 3). Both horizontal directions (L and T) show similar amplification patterns with peak amplitudes at about 0.9 Hz, whereas the vertical direction has the largest amplification at 1.85 Hz, nearly twice the horizontal peak vibration frequency. The peak SSR amplitudes at the fundamental vibration frequencies are about eight in the L, T, and vertical directions.

The SSR in the horizontal directions (Fig. 5(a,b)) show a second peak at about 3 Hz, which could be associated to the second harmonic mode of the earth structure. Note that the ratio between 3 Hz and the fundamental frequency at 0.9 Hz is about 3:1, similar to the ratio between the frequencies of the second and the first harmonics of a single horizontal soil layer predicted by the one-dimensional shear wave propagation theory (Roesset 1977).

Figure 6 shows examples of eHVSr computed for the stations T12, T13, and T14 located along a cross-section near the direction change of the crest axis (Fig. 2). The peak frequency of station T12 at the dam toe is 1.7 Hz with an average peak amplitude close to five (Fig. 6(a)). In contrast, the peak

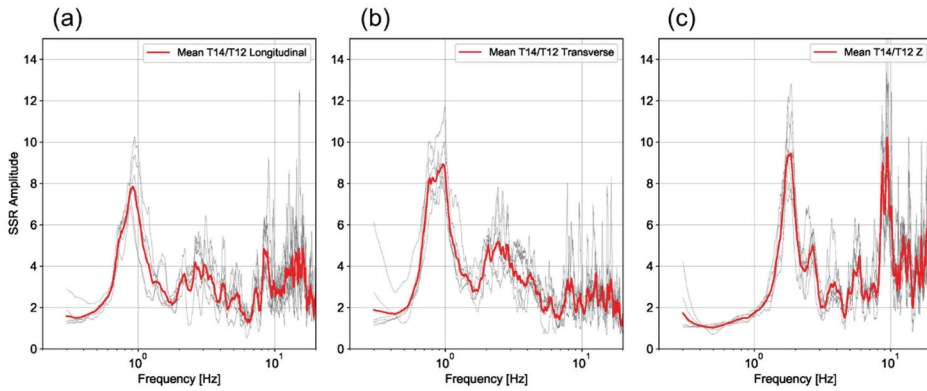


**Figure 5.** SSR computed for the station pair T14-T12 in the (a) longitudinal, (b) transverse, and (c) vertical directions.

frequency of the sensor T14 over the crest is 0.95 Hz with an average peak amplitude near seven (Fig. 6 (c)). This peak frequency is similar to that found in the SSR computed for the station pair T14-T12 in the longitudinal and transverse directions (Fig. 5(a,b)). The eHVSr of the sensor located in the downstream slope shows two peaks at about 0.9 and 1.1 Hz (Fig. 6(b)). The nature of these peaks will be addressed in the Discussion section.

Figure 7 shows mHVSr calculated in the same stations analyzed in Fig. 6. The shape of the curves, the peak frequencies and peak amplitudes are similar to those obtained with earthquake records. Moreover, the peak frequencies of the station in the crest T14 are similar to the frequencies found in the SSR (Fig. 5(a,b)). The second peak at about 3 Hz found in T14 (Fig. 7(c)) is similar to that found in the SSR of the same station (Fig. 5(a,b)), which could be associated to the second harmonic mode of the earth structure. The mHVSr at the station T13 also has two peaks around 1 Hz.

Figure 8 compares the average peak frequencies obtained from eHVSr and mHVSr for all the individual stations shown in Fig. 2(a). The results are shown for the transverse (filled symbols) and longitudinal directions (open symbols). Peak frequencies obtained from eHVSr and mHVSr in the crest and the downstream slope are similar in a wide range of frequencies between 0.8 and 1.6 Hz although eHVSr peak frequencies tend to exceed those from mHVSr. The larger variability in the peak frequencies obtained from eHVSr may be due to the few earthquakes analyzed compared to the

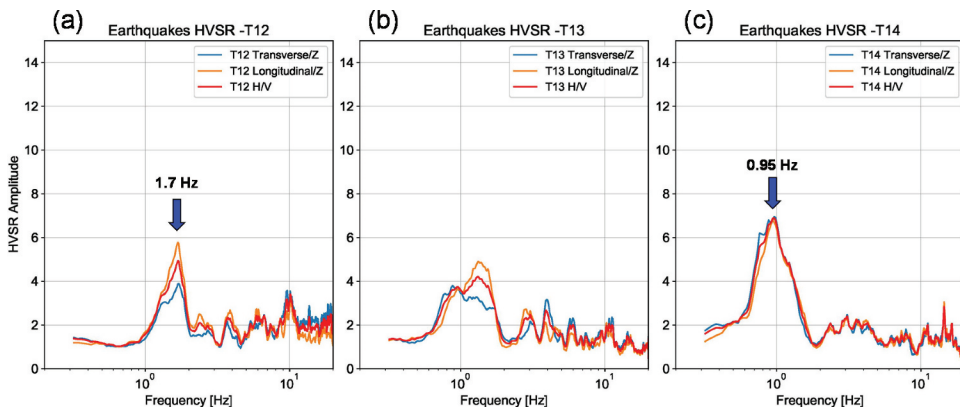


**Figure 6.** eHVSr computed for the stations (a) T12 (toe), (b) T13 (downstream slope), and (c) T14 (crest) in the T and L directions.

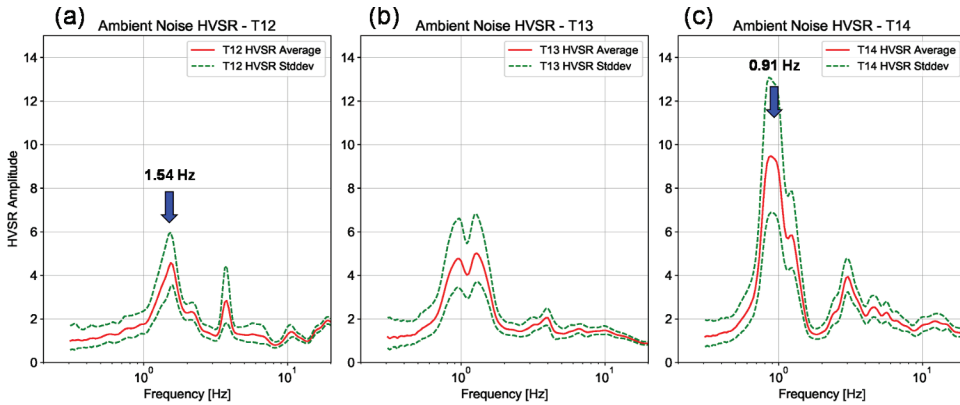


Figure 7. Average mHVSr computed for the stations (a) T12 (toe), (b) T13 (downstream slope), and (c) T14 (crest).

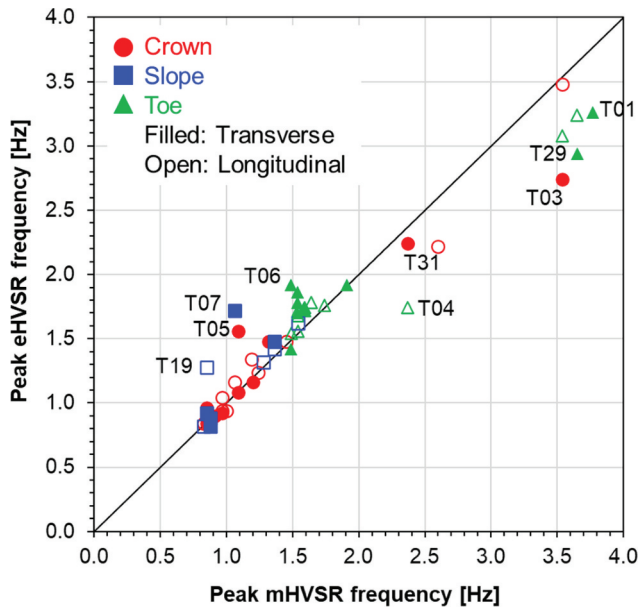


Figure 8. Comparison of peak frequencies of the seismic stations in Fig. 2 obtained from eHVSr and mHVSr.

longer records of seismic ambient noise considered for the calculation of mHVSr. Stations with two peaks in the SSR and HVSr (e.g. T05 and T19) and stations near the abutments (e.g. T01, T03, T04, T29, and T31) have the largest differences between eHVSr and mHVSr peak frequencies.

Figure 9 compares the peak frequencies obtained from SSR, mHVSr, and eHVSr for stations over the crest and the downstream slope. In general, the peak frequencies from the three methods agree in the frequency band between 0.8 and 1.6 Hz. The low correlation of the peak frequencies of station T13 in Fig. 9(a) is because this station has dual peaks. The correlation of the peak frequencies from eHVSr and SSR decreases in stations installed on the downstream slope (e.g. T07, T13, and T19 in Fig. 9(b)).

Stations near the abutments show lower correlation of the peak frequencies obtained from SSR and mHVSr (e.g. T05 and T28 in Fig. 9(a)). In these cases, the SSR do not show the peak frequencies predicted from mHVSr or eHVSr. For example, Fig. 10 compares the SSR, eHVSr, and mHVSr curves in the longitudinal and transverse directions at station T31. Although there are similarities

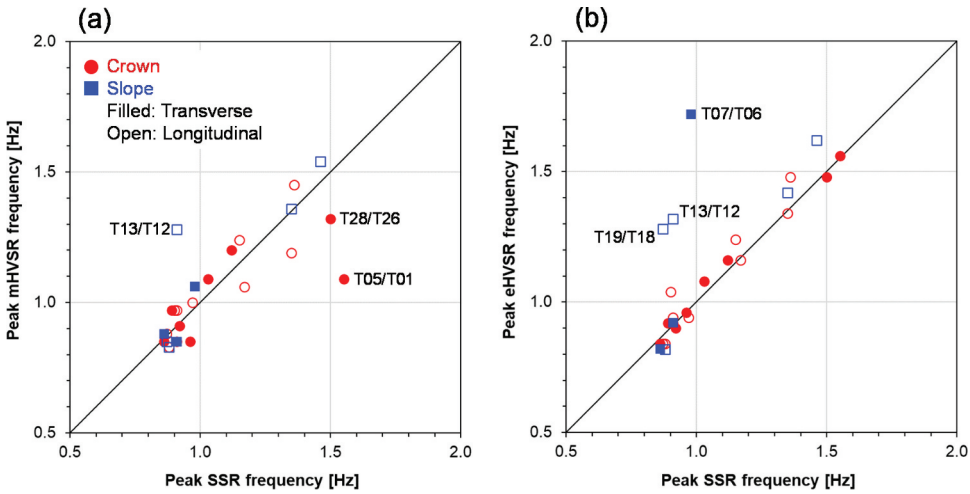


Figure 9. Comparison of peak frequencies of the seismic stations in Fig. 2 obtained from SSR with respect to (a) mHVSr and (b) eHVSr.

between eHVSr and mHVSr, both of them are different from the SSR. The difference could be related to the amplification pattern of the reference station (T29) used in the calculation of the SSR at station T31.

Figure 11(a) shows the variation of the peak frequency of mHVSr along the longitudinal embankment dam axis considering the distance from the north abutment. Stations at the dam toe over the foundation soil tend to have peak frequencies of about 1.5 Hz in the central part of the dam from 450 m to 1,900 m of the north abutment. Similarly, the peak frequencies of stations either along the crest or the downstream slope tend to have values between 0.9 and 1.1 Hz from 350 m to 1,500 m from the north abutment. The fundamental frequencies in stations in the crest and the dam toe increase

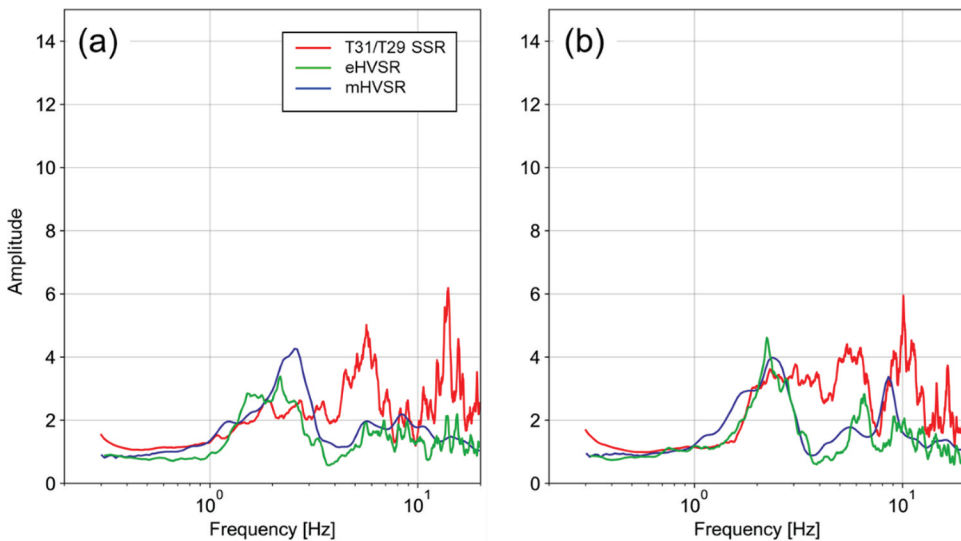
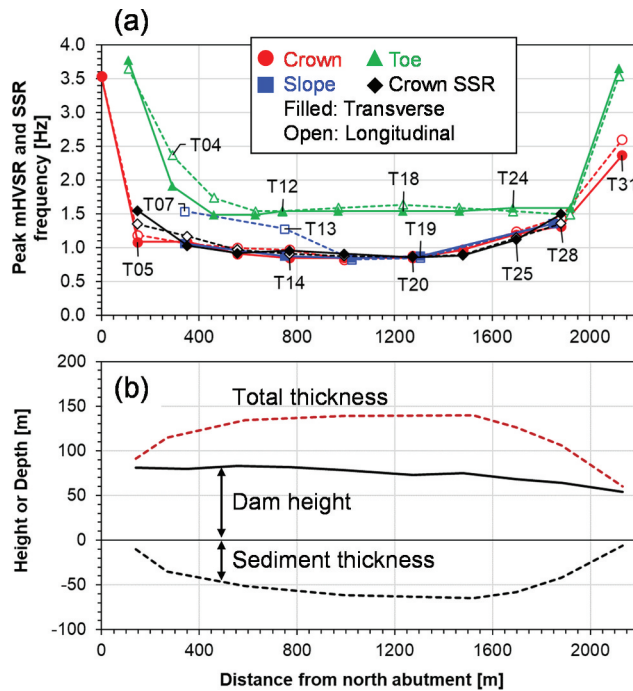


Figure 10. Comparison of the average SSR, eHVSr, and mHVSr in the (a) longitudinal and (b) transverse directions at station T31.



**Figure 11.** (a) Peak frequencies obtained from SSR and mHVSr evaluated in the crest, slope, and dam toe, compared to (b) the height of the embankment and the sediment thickness along the dam crest. Total thickness is the sum of the dam height and the sediment thickness.

drastically near the abutments. The figure also shows that the SSR peak frequencies in the central part of the dam agree with the mHVSr peak frequencies. Note that SSR of stations near the abutments are not presented in the figure.

## 6. Discussion

Figure 11 shows the changes in peak frequencies obtained from the mHVSr and SSR, as well as the dam height and the thickness of the foundation sediment along the dam crest. The sediment thickness in the foundation soil deposit was estimated from geological reports developed prior the construction of the tailings dam whereas the dam height was estimated from as-built blueprints. The somewhat constant fundamental vibration frequencies measured by the stations over the crest in the central part of the dam (from 350 m to 1,500 m of the north abutment) are related to a zone where the total thickness, calculated as the sum of the dam height and the sediment thickness, remains approximately constant at 140 m. A similar trend is observed in the frequencies calculated from the stations in the toe from 450 m to 1900 m of the north abutment. In contrast, the fundamental frequencies in stations near the abutments, both in the crest and the toe, increase drastically as the sediment thickness decreases. The peak frequencies in stations in the downstream slope are similar to those at the crest but some stations exhibit different peak frequencies in the longitudinal and transverse directions (e.g. T07 and T13).

The fundamental vibration frequency over the embankment dam is lower than that over the toe because the thickness of the underlying sediment at the toe is smaller than the material below the stations at the crest. In general, the amplitudes of the mHVSr and eHVSr in the crest are larger than the amplitudes at the toe (as shown in Figs. 6 and 7).

The fundamental frequencies of the stations installed over the foundation soil may be affected not only by the thickness of the foundation sediments but also by the interaction with the embankment dam. Decoupling these two effects may require further studies. The stations in the foundation soil

should be ideally installed at a further distance from the dam. We could not explore this issue due to constraints faced in the existing infrastructure and temporary works performed during the deployment of the temporal seismic array.

The eHVSR and mHVSR of the stations installed on the downstream slope show two peaks (e.g. Fig. 6(b) and Fig. 7(b)). A similar result was found for sloping terrains numerically analyzed with 2D and 3D finite-element simulations (Diaz-Segura 2016). The peak at the highest frequency seems to be associated to the fundamental frequency of the horizontal soil deposit that extend beyond the toe of the slope whereas the peak at the lowest frequency is seemingly related to the fundamental frequency of the horizontal soil deposit that extend beyond the crest of the slope. The amplitudes of both peaks vary along a slope cross-section, but the frequencies remain relatively constant. According to this study, a sloping terrain is better represented by a couple of dominant frequencies, instead of a single fundamental frequency.

The eHVSR retains most of the features of the mHVSR calculated from seismic ambient noise. In particular, the fundamental vibration frequencies are almost identical in both cases. This result suggests that the fundamental frequency of tailings dams can be recovered from earthquakes recorded by accelerometers, which is the most commonly installed type of sensor in these geo-structures (Campaña et al. 2016).

Figure 12(a) shows a shear-wave profile representative of the tallest dam section from the crest to the foundation soil (see Fig. 2(b)). The  $V_s$  profile follows the expression proposed by Gazetas (1982) for earth dams

$$V_s(z) = V_{sb} \left[ \frac{z+h}{H+h} \right]^{1/3}; \quad 0 < z < H \quad (1)$$

Where  $H = 85$  m is the height of the dam section (i.e. the height of a truncated wedge) and  $V_{sb} = 360$  m/s is the maximum shear-wave velocity at the base of the dam, considering a truncation ratio  $\lambda = h/(H+h) = 0.05$  ( $h = 4.475$  m is the distance from the truncated tip to the imaginary intersection between the downstream and upstream slopes of the wedge). The shallower 40 m of the  $V_s$ -profile in Fig. 12(a) fits the lower-bound velocities obtained from 30  $V_s$  profiles obtained with the MASW method and 7  $V_s$  profiles obtained from seismic cone penetration tests (sCPT) performed in the dam. The upper and lower bounds of these  $V_s$  profiles are shown in Fig. 12(a).

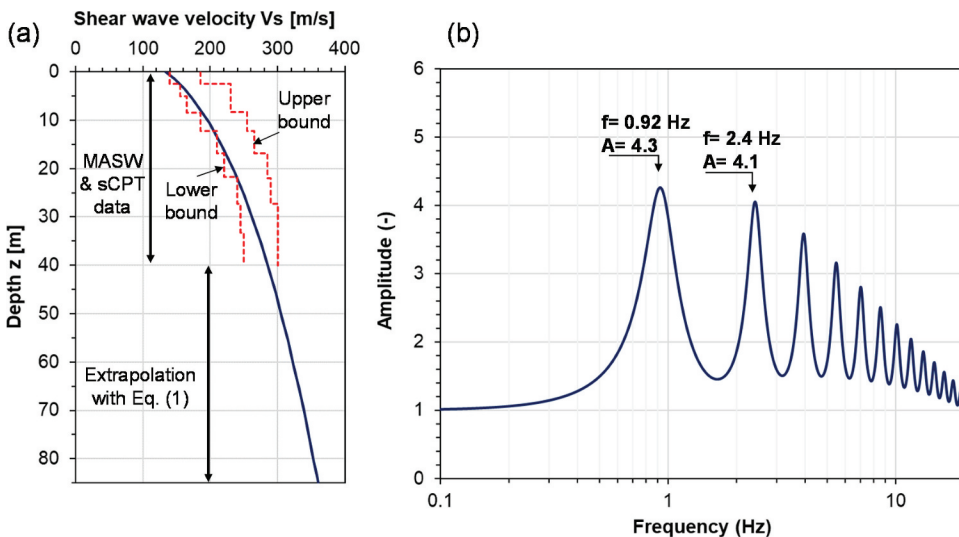
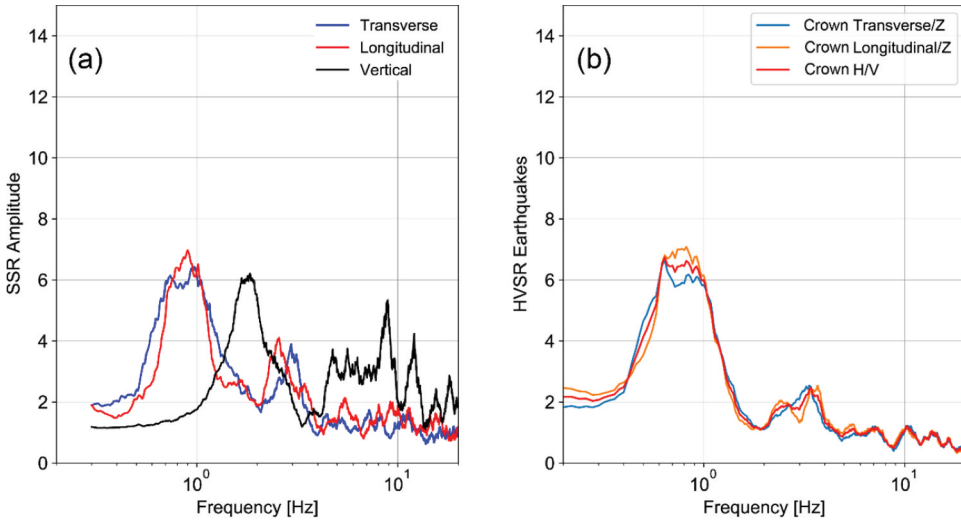


Figure 12. (a) Shear-wave velocity profile representative of the tallest section of the dam. (b) 1D SH-wave transfer function.



**Figure 13.** (a) SSR and (b) eHVSr at the dam crest calculated from records of the 2015 Illapel Earthquake. The location of the accelerometer is shown in Fig. 2(a).

Figure 12(b) shows the theoretical transfer function of a 1D soil column with the shear wave velocity profile shown in Fig. 12(a), a density of  $1.7 \text{ ton/m}^3$ , and a constant critical damping ratio of 2% when it is subjected to a vertically incident SH-wave (Roesset 1977). The model assumes that the substrate of the dam has a shear-wave velocity  $V_{sr} = 1,000 \text{ m/s}$ , a density of  $2.2 \text{ ton/m}^3$ , and a damping ratio of 2%. The fundamental frequency of the 1D model is  $f = 0.92 \text{ Hz}$ , similar to the frequencies found from SSR and HVSR around station T14 in the central part of the dam (see Figs. 5, 6, and 7). The amplitude of the theoretical transfer function is about half that of the empirical SSR.

On the other hand, for small values of the truncation ratio  $\lambda = h/(H+h)$ , the fundamental frequency of either a homogeneous or an inhomogeneous two-dimensional truncated wedge can be approximated by (Gazetas 1982)

$$f_0 = \frac{V_{sb}}{3(H+h)} \quad (2)$$

Evaluating Eq. 2 for  $H = 85 \text{ m}$ ,  $h = 4.475 \text{ m}$ , and  $V_{sb} = 360 \text{ m/s}$  yields a fundamental frequency  $f_0 = 1.34 \text{ Hz}$ .

These results suggest that the fundamental frequency of a tailings embankment dam with a gentle downstream slope, such as that analyzed in our study, may be estimated in the central part, away from the abutments, from the theoretical transfer function of a 1D soil column that extend from the dam crest to the foundation soil.

This preliminary conclusion may be valid for small magnitude earthquakes. To test its validity for larger earthquakes, we analyzed the records from the 2015 Mw 8.3 Illapel Earthquake gathered from GeoSig GSR AC-63 triaxial force balance accelerometers. The peak ground accelerations recorded in the crest sensor were  $0.11 \text{ g}$ ,  $0.09 \text{ g}$ , and  $0.07 \text{ g}$  in the transverse, longitudinal, and vertical directions, respectively. The peak ground accelerations recorded in the base sensor were  $0.05 \text{ g}$ ,  $0.06 \text{ g}$ , and  $0.03 \text{ g}$  in the transverse, longitudinal, and vertical directions, respectively. The location of the sensors in the crest and the base of the dam are shown in Fig. 2. Figure 13(a) shows SSRs obtained as the ratio between the signal in the crest and the base in the three directions. The fundamental frequencies obtained from the SSR are about  $0.9 \text{ Hz}$  in both horizontal directions and about  $1.8 \text{ Hz}$  in the vertical

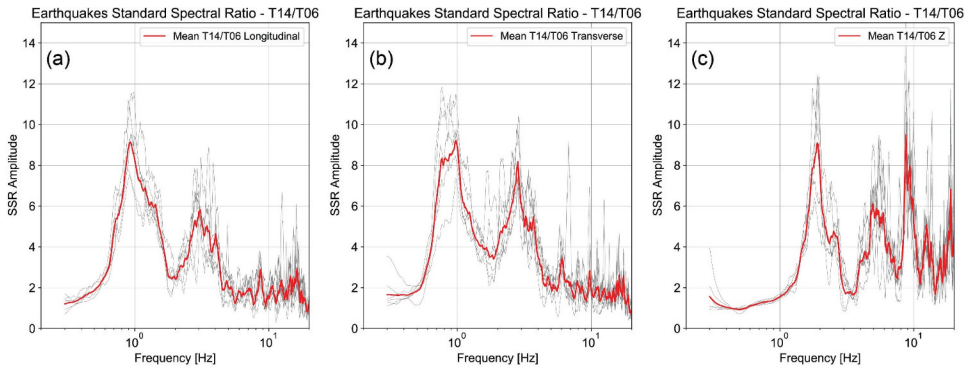


**Figure 14.** SSR computed for the station pair T14-T06 in the (a) longitudinal, (b) transverse, and (c) vertical directions.

direction. Similar horizontal fundamental frequencies are found processing the earthquake records as eHVSr (Fig. 13(b)). These values agree with the frequencies obtained in this study for the central part of the embankment from SSR and mHVSr (see Fig. 11(a)).

Since the accelerometers were not aligned in the same cross-section, we calculated SSR with the closest sensors to the accelerometers, T14 in the crest and T06 at the dam toe. Figure 14 shows the SSR obtained in the three directions. Results are similar to those obtained from the pair T14-T12 in Fig. 5.

Sources of differences between the SSR calculated from the 2015 Illapel Earthquake records are the height of the dam, 83 m in 2015 compared to 85 m in 2018, and slight nonlinear effects caused by larger strain levels induced by the earthquake. However, nonlinear effects may not be so pronounced as expected given the low peak accelerations recorded in the dam toe and the embankment.

## 7. Conclusions

The results from the mHVSr and eHVSr are consistent and show that the foundation soil is stiffer than the embankment dam, the fundamental vibration frequency of the dam is about 0.9 Hz in the central part away from the abutments, and there are differences in the vibration frequencies along cross-sections of the downstream slope and along the crest longitudinal axis from the north to the south abutment.

The results of the HVSr were compared with SSR calculated between the crest and the dam toe using the available earthquake records. Both methods are consistent in terms of the fundamental vibration frequencies and amplification factors.

The agreement between mHVSr, eHVSr, and SSR improves in the central part of the dam, approximately 400 m away from the abutments. We hypothesize that more complex seismic amplification patterns may develop near the abutments due to abrupt changes in the dam height and sediment thickness in the foundation soil. The difference between SSR and HVSr could help identifying zones of the dam that can be studied with a 2D approach, such as 2D numerical simulations, from zones near the abutments of the dam that must be analyzed with 3D methods.

The fundamental vibration frequency obtained from HVSr and SSR in the central part of the dam with gentle downstream slope can be fairly approximated by the value obtained from the 1D SH-wave propagation theory, considering a soil column from the dam crest to the interface with the foundation soil.

## Data Availability Statement

The data that support the findings of this study are available on request from the corresponding author, CP. The data are not publicly available due to privacy restrictions from the partner mining company involved in this study.

## Disclosure Statement

No potential conflict of interest was reported by the author(s).

## Funding

Support for this research was provided by the Advanced Mining Technology Center (AMTC PIA ANID grant AFB180004). César Pastén thanks the support from the ANID Fondecyt grant N° 1190995.

## References

- Bard, P.-Y., SESAME-Team. 2004. Guidelines for the implementation of the H/V Spectral Ratio technique on ambient vibrations measurements, processing and interpretation. European Commission – Research General Directorate.
- Borcherdt, R. D. 1970. Effects of local geology on ground motion near San Francisco Bay. *Bulletin of the Seismological Society of America* 60: 29–61.
- Campañá, J., E. Bard, C. Cano, and L. Valenzuela. 2016. Registro Sísmico en Depósito de Relaves. IX Congreso Chileno de Ingeniería Geotécnica, December 5 to 7, 2016, Valdivia, Chile.
- Cetin, K.O., N. S. Isik, S. Batmaz, and S. Karabiber. 2005. A comparative study on the actual and estimated seismic response of kiralkizi dam in Turkey. *Journal of Earthquake Engineering* 9 (4): 445–60. doi:10.1080/13632460509350550.
- Del Gaudio, V., S. Muscillo, and J. Wasowski. 2014. What we can learn about slope response to earthquakes from ambient noise analysis: An overview. *Engineering Geology* 182: 182–200. doi:10.1016/j.enggeo.2014.05.010.
- Diaz-Segura, E. G. 2016. Numerical estimation and HVSR measurements of characteristic site period of sloping terrains. *Geotechnique Letters* 6 (2): 176–81. doi:10.1680/jgele.16.00009.
- Dobry, R., and L. Alvarez. 1967. Seismic failures of Chilean Tailings Dams. *Journal of the Soil Mechanics and Foundations Division* 93 (6): 237–60. doi:10.1061/jsfeaq.0001054.
- Fernández, J., C. Pastén, S. Ruiz, and F. Leyton. 2019. Damage assessment of the 2015 Mw 8.3 Illapel earthquake in the North-Central Chile. *Natural Hazards* 96 (1): 269–83. doi:10.1007/s11069-018-3541-3.
- Gazetas, G. 1982. Shear vibration of vertically inhomogeneous earth dams. *International Journal for Numerical and Analytical Methods in Geomechanics* 6 (2): 219–41. doi:10.1002/nag.1610060208.
- Gazetas, G. 1987. Seismic response of earth dams: Some recent developments. *Soil Dynamics and Earthquake Engineering* 6 (1): 2–47. doi:10.1016/0267-7261(87)90008-X.
- He, J., S. Qi, Y. Wang, and C. Saroglou. 2020. Seismic response of the Lengzhuguan slope caused by topographic and geological effects. *Engineering Geology* 265: 105431. doi:10.1016/j.enggeo.2019.105431.
- Molnar, S., J. F. Cassidy, S. Castellaro, C. Cornou, H. Crow, J. A. Hunter, S. Matsushima, F. J. Sánchez-Sesma, and A. Yong. 2018. Application of microtremor horizontal-to-vertical spectral ratio (MHVSR) analysis for site characterization: State of the art. *Surveys in Geophysics* 39 (4): 613–31. doi:10.1007/s10712-018-9464-4.
- Nakamura, Y. 1989. A method for dynamic characteristics estimation of subsurface using microtremor on the ground surface. *Quarterly Report of Railway Technical Research Institute* 30: 25–33.
- Pastén, C., M. Sáez, S. Ruiz, F. Leyton, J. Salomón, and P. Poli. 2016. Deep characterization of the Santiago Basin using HVSR and cross-correlation of ambient seismic noise. *Engineering Geology* 201: 57–66. doi:10.1016/j.enggeo.2015.12.021.
- Roesset, J. M. 1977. Soil amplification of earthquakes. In *Numerical methods in geotechnical engineering*, ed. C. S. Desai and J. T. Christian, McGraw Hill, 639–52.
- Ruiz, S., and R. Madariaga. 2018. Historical and recent large megathrust earthquakes in Chile. *Tectonophysics* 733: 37–56. doi:10.1016/j.tecto.2018.01.015.
- Valenzuela, L. 2016. Design, construction, operation and the effect of fines content and permeability on the seismic performance of tailings sand dams in Chile. *Obras y proyectos* 19 (19): 6–22. doi:10.4067/S0718-28132016000100001.
- Verdugo, R., G. Peters, J. Campaña, L. Valenzuela, and E. Bard. 2017. Evaluation of tailings dams subjected to large earthquakes. Proceedings of the 19th International Conference on Soil Mechanics and Geotechnical Engineering, Seoul, Korea, 1615–18.
- Villavicencio, G., R. Espinace, J. Palma, A. Fourie, and P. Valenzuela. 2014. Failures of sand tailings dams in a highly seismic country. *Canadian Geotechnical Journal* 51 (4): 449–64. doi:10.1139/cgj-2013-0142.
- Wilkinson, J. J. 2013. Triggers for the formation of porphyry ore deposits in magmatic arcs. *Nature Geoscience* 6 (11): 917–25. doi:10.1038/ngeo1940.
- WISE Uranium Project. 2019. Chronology of major tailings dam failures, World Information Service on Energy Uranium Project, Accessed March 10, 2019, <http://www.wise-uranium.org/mdaf.html>